Wnt Inhibitory Factor 1 (*Wif1*) Is Regulated by Androgens and Enhances Androgen-Dependent Prostate Development

Kimberly P. Keil, Vatsal Mehta, Amanda M. Branam, Lisa L. Abler, Rita A. Buresh-Stiemke, Pinak S. Joshi, Christopher T. Schmitz, Paul C. Marker, and Chad M. Vezina

Departments of Comparative Biosciences (K.P.K., V.M., L.L.A., P.S.J., C.T.S., C.M.V.) and Pharmaceutical Sciences (A.M.B., R.A.B.-S., P.C.M.) and the Molecular and Environmental Toxicology Center (A.M.B.), University of Wisconsin-Madison, Madison, Wisconsin 53706

Fetal prostate development from urogenital sinus (UGS) epithelium requires androgen receptor (AR) activation in UGS mesenchyme (UGM). Despite growing awareness of sexually dimorphic gene expression in the UGS, we are still limited in our knowledge of androgen-responsive genes in UGM that initiate prostate ductal development. We found that WNT inhibitory factor 1 (*Wif1*) mRNA is more abundant in male *vs.* female mouse UGM in which its expression temporally and spatially overlaps androgen-responsive steroid 5α-reductase 2 (*Srd5a2*). *Wif1* mRNA is also present in prostatic buds during their elongation and branching morphogenesis. Androgens are necessary and sufficient for *Wif1* expression in mouse UGS explant mesenchyme, and testicular androgens remain necessary for normal *Wif1* expression in adult mouse prostate stroma. WIF1 contributes functionally to prostatic bud formation. In the presence of androgens, exogenous WIF1 protein increases prostatic bud number and UGS basal epithelial cell proliferation without noticeably altering the pattern of WNT/β-catenin-responsive *Axin2* or lymphoid enhancer binding factor 1 (*Lef1*) mRNA. *Wif1* mutant male UGSs exhibit increased (*Sfrp*)*2* and (*Sfrp*)*3* expression and form the same number of prostatic buds as the wild-type control males. Collectively our results reveal *Wif1* as one of the few known androgen-responsive genes in the fetal mouse UGM and support the hypothesis that androgen-dependent *Wif1* expression is linked to the mechanism of androgen-induced prostatic bud formation. **(*Endocrinology* 153: 6091–6103, 2012)**

Androgens initiate prostatic bud formation from the urogenital sinus (UGS) and stimulate prostatic bud elongation, ductal branching morphogenesis, and differentiation of mature prostatic ductal epithelium (1, 2). During fetal prostate development, androgens activate androgen receptors (ARs) in UGS mesenchyme (UGM) to induce prostatic bud formation in UGS epithelium (UGE) (1, 3–5). The developing prostate has therefore been used as a model to assess the role of androgens in mesenchymal/epithelial interactions. A longstanding question in the prostate development field is how ARs in UGM communicate with UGE to establish the pattern and quantity of prostatic buds that will form. Continued investigation is expected to shed light on how the developing prostate microenvironment influences prostate epithelial cell fate. It may also elucidate how adult prostate stromal ARs reactivate developmental signaling pathways to cause inappropriate proliferative growth during prostate disease (6–13).

Numerous gene expression profiling studies have been conducted to identify androgen-responsive mRNAs in fe-

ISSN Print 0013-7227 ISSN Online 1945-7170
Printed in U.S.A.

doi: 10.1210/en.2012-1564 Received May 24, 2012. Accepted September 24, 2012.
First Published Online October 18, 2012

Abbreviations: ACTA2, Smooth muscle actin-α2; AR, androgen receptor; CDH1, cadherin 1; DAPI, 4′,6-diamidino-2-phenylindole, dilactate; 3dC, 3-d castrated males; DHT, 5α-dihydrotestosterone; 3dS, 3-d sham-castrated controls; E, embryonic day; GUDMAP, GenitoUrinary Development Molecular Anatomy Project; IHC, immunohistochemistry; ISH, *in situ* hybridization; KRT14, keratin 14; *Lef1*, lymphoid enhancer binding factor 1; LUT, lower urinary tract; O.C.T., optimal cutting temperature; OHF, hydroxyflutamide; P, postnatal day; PH3, phosphohistone H3; *Sfrps*, secreted frizzled related proteins; *Srd5a2*, steroid 5α-reductase 2; UGE, UGS epithelium; UGM, UGS mesenchyme; UGS, urogenital sinus; WIF1, WNT inhibitory factor 1.

tal prostate (14–18). The WNT pathway has been identified as a major androgen-responsive pathway in developing UGS and many *Wnt*s are more abundant in male compared with female mouse UGS (14, 15, 19). Several WNT antagonists are also present during prostate development, including but not limited to WNT inhibitory factor 1 (*Wif1*) and secreted frizzled related proteins (*Sfrps*) *1* and *-2* (14, 15, 20). Tight regulation of WNT signaling is required for the normal program of prostatic branching morphogenesis (20, 21).

Despite growing awareness of sexually dimorphic gene expression in the UGS, we are still limited in our knowledge of androgen responsive genes in UGM that initiate prostate ductal development. We conducted a high-throughput *in situ* hybridization (ISH) screen in conjunction with the GenitoUrinary Development Molecular Anatomy Project (GUDMAP) to resolve developing prostate molecular anatomy and identify candidate androgen-responsive mRNAs in fetal mouse UGM (www.gudmap.org). Because mesenchymal AR signaling is necessary for prostate development, we screened for mRNAs present in fetal male UGM during prostatic bud formation at embryonic day (E) 17.5 and absent, less abundant, or differently patterned in E17.5 female UGM. Our screen revealed a sexually dimorphic expression pattern for the secreted WNT-binding protein *Wif1*, which was more abundant in male compared with female UGM. In this manuscript, we tested hypotheses that androgens are necessary and sufficient for *Wif1* mRNA expression in developing and sexually mature mouse prostate and that exogenous WIF1 protein increases androgen-dependent prostatic bud formation in UGS explant cultures. Our results reveal *Wif1* as one of the first androgen induced enhancers of prostatic bud formation and thereby provide new insight into the mechanism of androgen action during mouse prostate development.

Materials and Methods

Animals

Wild-type C57BL/6J mice were purchased from Jackson Laboratory (Bar Harbor, ME). *Wif1*^{tm1Dmth} targeted mutant mice (*Wif1*^{lacZ}) (22) were from Dr. Igor Dawid (*Eunice Kennedy Shriver* National Institute of Child Health and Human Development, Bethesda, MD) and were maintained on a C57BL/6J × 129/SV background. Mice were housed in polysulfone cages containing corn cob bedding and maintained on a 12-h light, 12-h dark cycle at 25 ± 5 C and 20–50% relative humidity. Feed (Diet 2019 for males and Diet 7002 for pregnant females; Harlan Teklad, Madison, WI) and water were available *ad libitum*. All procedures were approved by our institutional Animal Care and Use Committee and conducted in accordance with the National Institutes of Health Guide for the Care and Use of Laboratory Animals. To obtain timed-pregnant dams, females were paired overnight with males. The next morning was considered E0.5. Dams were euthanized by CO_2 asphyxiation. *Wif1* embryos were genotyped with PCR primers for wild-type allele (5′-CG AGAACTTCACAAGCAGCACAGG-3′, and 5′-CCTGTTAC AAATCTGCAGTCAGG-3′, 500 bp) and mutant allele (5′-CT GTGGCCGGCTGGGTGTGGCGG-3′and5′-AGCACTCTAG CCTGATGGGCTC-3′, 500 bp). For *in vivo* experiments, wild-type timed pregnant dams were injected on E13.5 and E14.5 or E17.5 and E18.5 with sterile corn oil (5 ml/kg sc maternal dose) containing 10% ethanol alone or containing flutamide (200 mg/kg · d maternal dose; no. F9397-1G; Sigma, St. Louis, MO). UGSs were collected at E15.5 and postnatal day (P) 0.

Assay for β-galactosidase activity

LacZ-dependent β-galactosidase activity was assessed as described previously (19).

Castration and testosterone treatment

Forty-eight- to fifty-d-old adult male wild-type mice were given buprenorphine (0.1 mg/kg) for analgesia and isoflurane (1–2% inhalant) for anesthesia. A scrotal incision was made, the testes and associated fat pads were externalized, ligated, and excised, and the incision was closed with a suture. Sham castrations were performed as described above except testes and fat pads were not ligated or removed. Some mice received 1 cm SILASTIC brand (Dow Corning, Midland MI) capsule implants (empty or testosterone filled), which were engineered in our laboratory from SILASTIC brand tubing (1.57 mm inside diameter, 3.18 mm outside diameter,) and inserted into the sc space above the scapular fat pad.

In situ hybridization

To allow for ISH comparisons between males and females and among treatment or genotypic groups, tissues from each comparison group were dissected, fixed, dehydrated, and stored under identical conditions. Tissues were processed for ISH at the same time and in the same vessel so qualitative comparisons could be made among or between groups. UGSs were fixed overnight in 4% paraformaldehyde and stained in whole mount, cut with a vibrating microtome into 50 μm sections, or frozen in optimal cutting temperature (O.C.T.) medium and cut with a cryotome into 10-μm sections. Fresh adult prostate was frozen in O.C.T. medium and cut with a cryotome into 10-μm sections. PCR-based riboprobe synthesis (www.gudmap.org) and ISH on vibrating microtome-cut sections and UGS whole mounts are described elsewhere (23, 24) (www.gudmap.org). Primer sequences for generating PCR-based riboprobes are listed in Supplemental Table 1, published on The Endocrine Society's Journals Online web site at http://endo.endojournals.org. For ISH of frozen tissue sections, tissues were embedded in O.C.T. medium, frozen, sectioned, air dried for 10 min, and fixed for 1 h in PBS containing 4% paraformaldehyde. ISH was conducted as described previously (23) with the following modifications. Washes were conducted in slide mailer tubes with constant agitation. Tissues were permeabilized for 8 min at room temperature with 5 μg/ml Proteinase K. Slides were coverslipped and placed in a humidified hybridization chamber for prehybridization, probe, and antibody solution incubations. The hybridization solution was supplemented with 5% dextran sulfate. The

duration of all previously described washes (23) was reduced by half. BM Purple alkaline phosphatase precipitating chromagen (Roche Diagnostics, Indianapolis, IN) was used for detection of digoxigenin-labeled riboprobes. Incubation times were identical for all samples within a comparison group and staining times for each riboprobe are indicated in figure legends. For some UGS explants, light micrographs of BM Purple-stained tissue sections were captured, inverted, pseudocolored green, and merged with immunofluorescent images. The staining pattern for all the riboprobes was assessed in at least two tissue sections from at least two litter-independent mice. Gene expression patterns were annotated using the GUDMAP anatomical ontology.

Organ culture

E14.5 wild-type male and female UGSs were placed on 0.4-μm Millicell-CM filters (Millipore, Billerica, MA) and cultured for 1 or 4 d as described previously (25). Media were supplemented with 5α-dihydrotestosterone (DHT; 10 nM), hydroxyflutamide (OHF; 10 nM) (Sigma-Aldrich, St. Louis, MO) and/or recombinant human WIF1 protein (0–2000 ng/ml; R&D Systems, Minneapolis, MN). Media and supplements were changed every 2 d.

Immunohistochemistry (IHC)

Immunofluorescent staining of ISH-stained, frozen, paraffin, and vibrating microtome sections was performed as described previously (19, 26). Primary antibodies were diluted as follows: 1:200 rabbit anticadherin 1 (CDH1; 3195, Cell Signaling Technology, Beverly, MA), 1:250 mouse anti-smooth muscle actin-α2 (ACTA2; Leica Microsystems, Buffalo Grove, IL), 1:250 rabbit antiphospho-histone H3 (PH3; 9701s; Cell Signaling Technology) and 1:50 mouse anti-keratin 14 (KRT14; ms-115-p0; Thermo Scientific, Waltham, MA). Secondary antibodies were diluted as follows: 1:250 Dylight 549-conjugated antirabbit IgG (111-507-003; Jackson ImmunoResearch Laboratories, West Grove, PA) and Dylight 488-conjugated goat antimouse IgG (115-487-003; Jackson ImmunoResearch Laboratories). Immunofluorescently labeled tissues were counterstained with 4′,6-diamidino-2-phenylindole, dilactate (DAPI) and mounted in antifade media (PBS containing 80% glycerol and 0.2% *n*-propyl gallate).

RNA isolation and real-time RT-PCR

E17.5 UGE was enzymatically and mechanically separated from UGM and homogenized as described previously (25). RNA was purified with the Illustra RNAspin minikit (GE Healthcare, Pittsburgh, PA) and reverse transcribed with the SuperScript III first-strand synthesis system (Invitrogen, Carlsbad, CA). Real-time PCR was performed in 10.5-μl reactions containing 1× SsoFast EvaGreen Supermix (Bio-Rad Laboratories, Hercules, CA), 0.48 μM PCR primers, and 3.75 μl cDNA and amplified using the CFX96 PCR machine (Bio-Rad Laboratories). PCR primers were as follows: *Wif1*, 5′-GAG AAA GCC CTG TGC ATA CC-3′ and 5′-ACT GCT CTC TCC CTC GAG TCC-3′; *Krt14*, 5′-AAT TCT CCT CTG GCT CTC AGT CAT CC-3′ and 5′-AGC TTT AGT TCT TGG TGC GCA GGA C-3′; *Acta2*, 5′-CTG CCG AGC GTG AGA TTG-3′ and 5′-AAT GAA AGA TGG CTG GAA GAG AG-3′; and peptidyl prolyl isomerase a (*Ppia*), 5′-TCT CTC CGT AGA TGG ACC TG-3′ and 5′-ATC ACG GCC GAT GAC GAG CC-3′. Relative mRNA abundance was determined by the ΔC_t method as described previously (27) and normalized to *Ppia* abundance.

Statistical analyses

For RT-PCR, three tissue pools consisting of two to three UGSs per pool were used to measure mRNA abundance. For prostatic bud counting, UGSs were stained by ISH for NK3 homeobox 1 (*Nkx3-1*) mRNA and three individuals, blinded to treatment conditions, counted the total number of *Nkx3-1* positive prostatic buds in each of at least four UGSs per experimental group. *Nkx3-1* stained urethral gland buds were excluded from analysis (26). For immunolabeled cell counting, PH3-positive, KRT14-positive and double-positive cells were counted in at least two sections per UGS in at least three UGSs per treatment group. For the assessment of castration efficiency, lower urinary tract (LUT; including prostate, urethra, bladder, and seminal vesicle) wet weight was measured relative to body weight at time of euthanasia. Statistical analysis was performed using R version 2.13.1. Homogeneity of variance was determined using a Bartlett's test. A Student's *t* test or ANOVA, followed by Fisher's least significant difference test were used to identify significant differences ($P \leq 0.05$) between or among treatment groups.

Results

Demonstration of *Wif1* riboprobe specificity

We created a *Wif1* riboprobe and demonstrated its ability to recapitulate the *Wif1* expression pattern reported previously for a different *Wif1* riboprobe (28) in E13.5 mouse handplate mesenchyme (Supplemental Fig. 1A). To further establish selectivity of our riboprobe, we showed that the *Wif1* expression pattern in mouse UGS as revealed by ISH (described in the section below) was similar to the *lacZ* expression pattern in *Wif1*$^{lacz/+}$ UGS (Supplemental Fig. 1B).

Wif1 mRNA is more abundant in male compared with female UGM and overlaps androgen-responsive *Srd5a2* mRNA from the earliest stages of mouse prostate development

Our next objective was to analyze the *Wif1* expression pattern over a broad developmental period to include stages E14.5 to P5. This period spans the four earliest stages of prostate ductal development: prostatic bud specification, when molecular signals specify where prostatic buds will form from UGE (E14.5–16.5); prostatic bud initiation, when buds first project from UGE (E16.5–18.5); prostatic bud elongation, when prostatic buds extend into UGS stroma and prostatic ductal branching morphogenesis (E16.5 to P5) (1, 29, 30).

Fetal and neonatal mouse UGS sections were stained by ISH to visualize *Wif1* mRNA. To determine whether *Wif1* expression in mouse UGS is associated with AR activity, we compared its temporal and spatial expression to a

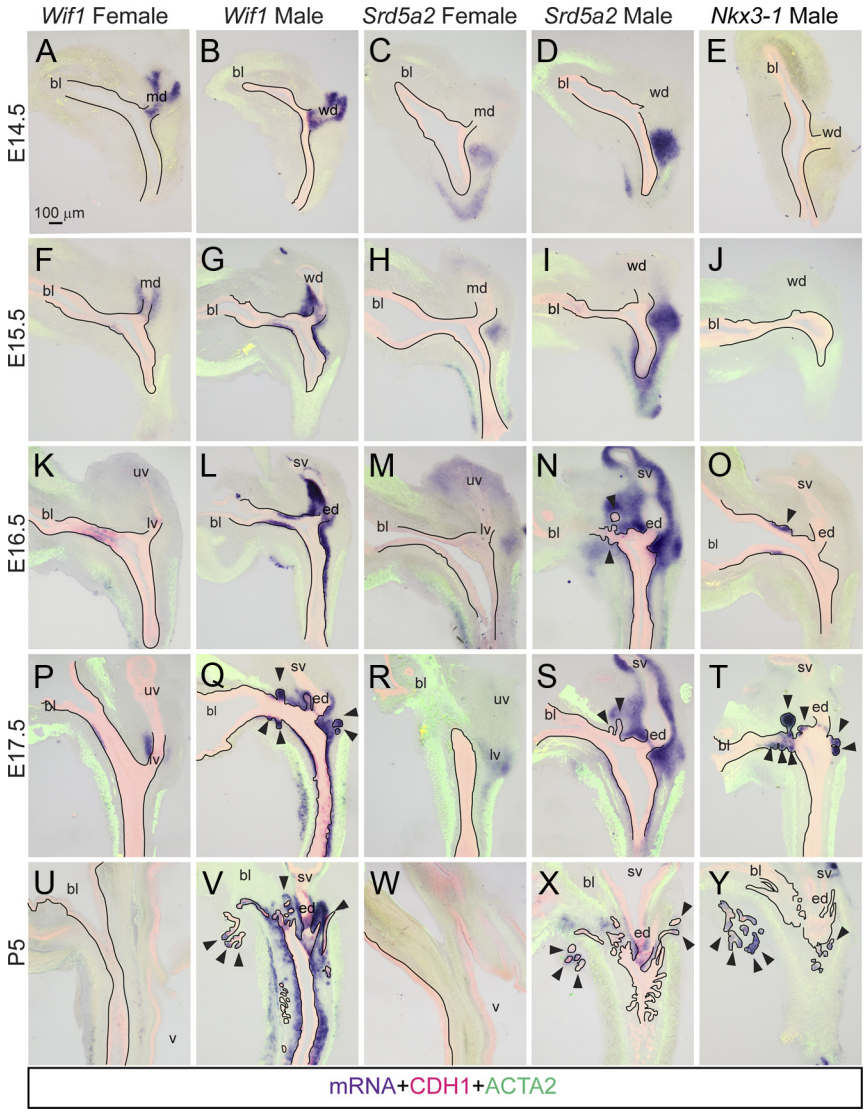

FIG. 1. *Wif1*, *Srd5a2*, and *Nkx3-1* mRNA expression in developing male and female mouse UGS. A–Y, Near midsagittal sections (50 μm) of E14.5 to P5 male and female UGSs were stained by ISH to visualize mRNA expression (*purple*) of *Wif1*, *Srd5a2* (marker of prostatic stromal AR activity), and *Nkx3-1* (marker of prostatic buds). Sections were then immunofluorescently stained with antibodies against CDH1 (*red*) to label all epithelium, and ACTA2 (*green*) present in mesenchyme. Results are representative of three litter-independent samples for each gender and stage. bl, Bladder; ed, ejaculatory duct; lv, lower vagina; md, Müllerian duct; sv, seminal vesicle; uv, upper vagina; v, vagina; wd, Wolffian duct. *Arrowheads* indicate prostatic buds. A *black line* marks the interface between UGS epithelium and mesenchyme. BM Purple detection time was the same for males and females and was as follows: *Wif1* (62 h), *Srd5a2* (31 h), *Nkx3-1* (47 h).

known androgen-responsive gene, *Srd5a2* (steroid 5α-reductase 2) (26, 31). To determine whether *Wif1* is present in UGS before prostatic specification, we compared its temporal expression pattern with the earliest known mRNA marker of the mouse prostate field, *Nkx3-1* (24, 32). To determine the onset and duration of sexually dimorphic *Wif1* mRNA expression, we compared its expression in male and female UGS at all examined developmental stages (Fig. 1). Tissues were also stained by IHC to visualize epithelium with CDH1 (*red*) and ACTA2 (*green*) so that *Wif1* expression could be assessed and described in the context of other tissue compartments (26).

Wif1 mRNA was detected in male and female UGS at E14.5, before prostate field specification as noted by the absence of *Nkx3-1* expression (Fig. 1, A–E). *Wif1* was more abundant in male compared with female UGS stroma beginning at E15.5 (Fig. 1, F and G) and continuing until at least P5 (Fig. 1, U and V). Intriguingly, the onset and duration of sexually dimorphic *Wif1* expression in UGS stroma coincided temporally with onset and duration of sexually dimorphic *Srd5a2* mRNA expression in UGS stroma (Fig. 1, H and I). Beginning at E15.5 and continuing until at least P5, *Wif1* and *Srd5a2* mRNAs were particularly concentrated in male urethral lamina propria mesenchyme (Fig. 1). This stromal subcompartment, positioned between UGE (labeled by CDH1, Fig. 1, *red*) and urethral muscularis propria (labeled by ACTA2, Fig. 1, *green*) (Fig. 1) (26), was previously identified as a key site of AR action during prostate development (33). *Wif1* also exhibited sexually dimorphic expression in UGE. Beginning at E16.5 and continuing until at least P5, *Wif1* was coexpressed with *Nkx3-1* in male UGS and prostatic bud epithelium (Fig. 1). *Wif1* was also detected in the male Wolffian duct, seminal vesicle, and ejaculatory duct mesenchyme between E14.5 to P5 and in urethral smooth muscle between stages E16 and P5. In female UGS, *Wif1* localized to lower vagina (sinus vagina) mesenchyme and to a discrete population of ventral urethral basal epithelium (Fig. 1, F, K, and P). The latter is an anatomical region in which the small *Nkx3-1*-positive epithelial buds have been documented in female C57BL/6J mouse fetuses (34). Collectively these results reveal localized *Wif1* expression in androgen-responsive male UGS stroma and in epithelial bud structures of male and female UGS.

To confirm ISH results showing *Wif1* is more abundant in male *vs.* female UGS, cDNA from microdissected E17.5 male and female UGE and UGM was analyzed by real-time PCR. We confirmed the purity of each cDNA preparation

by demonstrating selective expression of *Acta2* mRNA in the UGS mesenchymal cDNA preparation and *Krt14* in the UGS epithelial cDNA preparation (Supplemental Fig. 1C). We then demonstrated that *Wif1* mRNA was more abundant in male compared with female UGM and UGE (Supplemental Fig. 1C). Taken together, these results reveal that *Wif1* is present in the fetal mouse UGS in which it is more abundant in male compared with female fetuses.

Androgens are necessary and sufficient for *Wif1* mRNA expression in fetal mouse prostate mesenchyme

Prostate development requires AR activation in UGM (4, 5). The observation that *Wif1* is more abundant in male compared with female UGM, coupled with the fact that *Wif1* expression overlaps spatially and temporally with androgen-responsive *Srd5a2*, raised the hypothesis that *Wif1* mRNA expression in UGM is regulated by androgens. We assessed whether androgens are necessary for *Wif1* mRNA expression in UGM before prostatic bud formation (E14.5), remain necessary after prostatic bud initiation (E17.5), and are sufficient for *de novo Wif1* expression in E17.5 female UGM. The E14.5 male and E17.5 male and female UGSs were incubated for 24 h in organ culture media containing DHT and either vehicle alone or vehicle containing the AR antagonist OHF. After the culture period, UGSs were stained by ISH to visualize *Wif1* mRNA (pseudocolored green) and by IHC with anti-CDH1 (red, all epithelium) and DAPI (blue) to localize *Wif1* mRNA expression.

Androgen-responsive *Srd5a2* mRNA (26) was also visualized to confirm pharmacological sufficiency of AR agonist and antagonist treatments. In male UGSs, OHF treatment noticeably reduced *Srd5a2* and *Wif1* abundance in UGM but not in prostatic bud epithelium (Fig. 2, A–J, *insets*). In female UGSs, DHT treatment activated *Srd5a2* and *Wif1* expression specifically in UGM, and this action was blocked by OHF (Fig. 2, E, F, K, and L, *insets*). To independently confirm the requirement of androgens for *Wif1* expression in UGM, timed pregnant dams were dosed with AR antagonist flutamide before prostatic bud

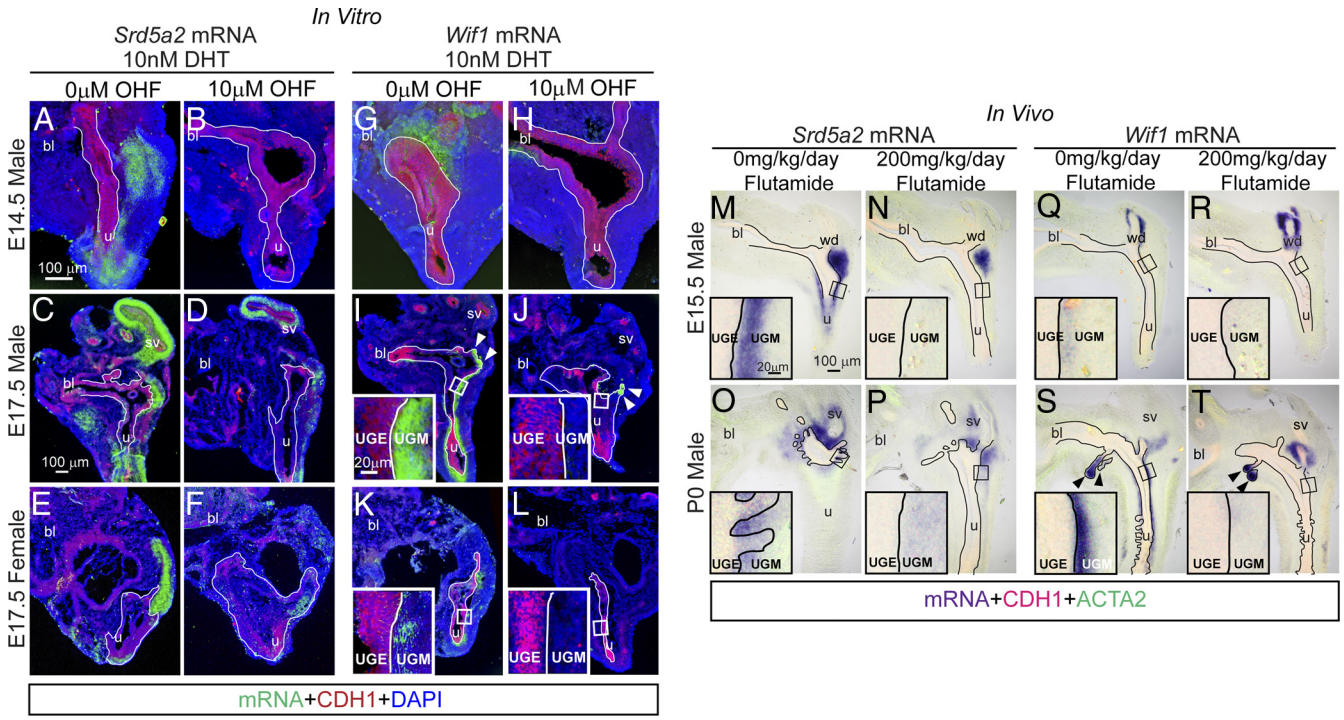

FIG. 2. AR signaling is necessary and sufficient for *Wif1* mRNA expression in fetal mouse prostate stroma. A–L, E14.5 male or E17.5 male and female UGS explants were cultured for 24 h in media containing DHT (10 nM) or DHT and the AR antagonist OHF (10 μM). Near midsagittal frozen sections (10 μm) were stained by ISH to visualize *Srd5a2* (A–F) and *Wif1* (G–L) mRNAs (*green*). Sections were then immunofluorescently stained with anti-CDH1 (*red*) antibody to label all epithelium and DAPI (*blue*). M–T, Timed pregnant dams were dosed with corn oil alone or corn oil containing flutamide on E13.4 and E14.5 and male UGSs collected on E15.5 or dosed on E17.5 and E18.5 and male UGSs collected on P0. Near midsagittal sections (50 μm) were stained by ISH to visualize *Srd5a2* (M–P) and *Wif1* (Q–T) mRNAs (*purple*). Sections were then immunofluorescently stained with anti-CDH1 (*red*) antibody to label all epithelium and anti-ACTA2 (*green*) to label smooth muscle. *Insets* represent magnified images. Results are representative of three litter-independent samples per treatment group and were processed as a single experimental unit. bl, Bladder; sv, seminal vesicle; u, urethra; wd, Wolffian duct. *Arrowheads* indicate presence of epithelial *Wif1* in prostatic buds. A *white* or *black line* marks the interface between UGS epithelium and mesenchyme. BM Purple detection time was the same for all samples across experimental groups and was as follows: *Wif1* (97 h, 10 μm frozen sections; 22 h, 50 μm sections); *Srd5a2* (97 h, 10 μm frozen sections; 22 h, 50 μm sections).

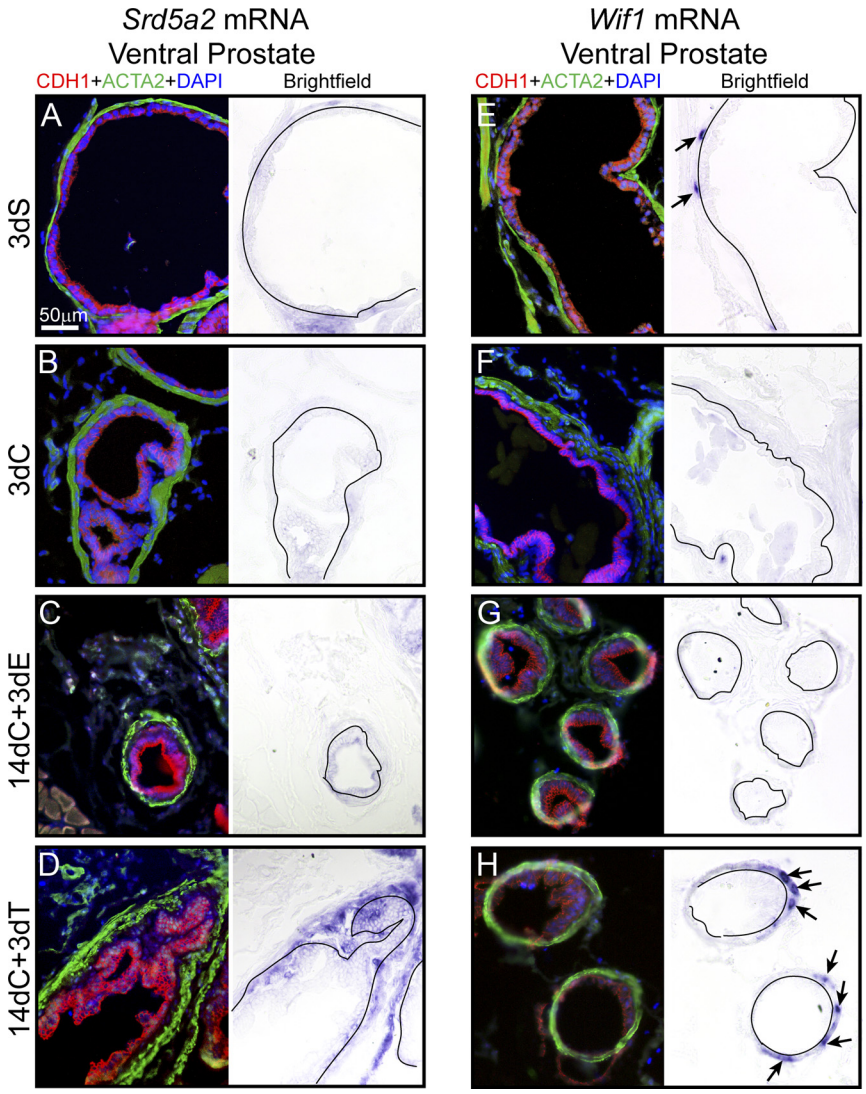

FIG. 3. AR signaling is necessary for *Wif1* mRNA expression in mature prostate stroma. Adult male mice (48–50 d) were castrated or sham castrated. Prostate tissue was obtained from some mice 3 d after sham castration (3dS) or 3 d after castration (3dC), whereas other mice received empty (14dC+3dE) or testosterone-filled (14dC+3dT) SILASTIC brand capsule implants (Dow Corning) 14d after castration and prostate tissue was obtained 3 d later. ISH was used to visualize *Srd5a2* (A–D) and *Wif1* (E–H) mRNA expression in frozen ventral prostate sections (10 μm). ISH sections were then immunofluorescently labeled with antibodies against CDH1 (*red*) to label all epithelium, ACTA2 (*green*) to label smooth muscle and DAPI (*blue*). Results are representative of three litter-independent samples per treatment group. *Arrows* represent *Wif1* mRNA-positive muscle cells. A *black line* marks the interface between UGS epithelium and stroma. BM Purple detection time was the same for all samples across experimental groups and was as follows: *Wif1* (75 h), *Srd5a2* (75 h).

formation (E13.5 and E14.5) or during prostatic bud formation (E17.5 and E18.5). Male UGSs were collected on E15.5 and P0 and stained by ISH to visualize *Wif1* and *Srd5a2* mRNA (purple) and by IHC with anti-CDH1 (red, all epithelium) and anti-ACTA2 (green, smooth muscle) (Fig. 2, M–T). Flutamide treatment noticeably reduced *Srd5a2* and *Wif1* abundance in male UGM (Fig. 2, M–T, *insets*) but not *Wif1* abundance in male prostatic bud epithelium (Fig. 2, S and T, *arrowheads*). These results support the hypothesis that androgens and active AR signaling are necessary and sufficient for *Wif1* mRNA expression in fetal UGM but not UGE.

Androgens are necessary and sufficient for *Wif1* expression in the adult mouse prostate stroma

We next tested whether androgens are necessary for *Wif1* expression in adult prostate stroma. Male mice were either sham castrated (control) or castrated to reduce circulating androgens and induce prostate involution. There was a significant reduction in relative LUT wet weight among 3-d castrated males (3dC) compared with 3-d sham-castrated controls (3dS; Supplemental Fig. 2). Tissues were stained by ISH to visualize *Srd5a2* and *Wif1* mRNA (purple) and by IHC with anti-CDH1 (red), anti-ACTA2 (green) and DAPI (blue) to localize mRNA expression. *Srd5a2* and *Wif1* mRNAs were detected in ventral prostate stroma of both experimental groups, but both mRNAs were visibly less abundant in 3dC *vs.* 3dS (Fig. 3, A, B, E, and F). We observed a similar trend in other prostate lobes and in seminal vesicle (Supplemental Fig. 3). These results suggest a testicular androgen requirement for normal *Wif1* mRNA expression in adult mouse prostate stroma.

We next tested whether exogenous androgen would restore *Wif1* expression in castrated mouse prostate stroma. Fourteen-day castrated mice were implanted with empty or testosterone-filled SILASTIC brand capsules (Dow Corning) and 3 d later were euthanized. Relative LUT wet weight was significantly greater among 14-d castrated males implanted with testosterone capsules (14dC+3dT) than among males implanted with empty capsules (14dC+3dE; Supplemental Fig. 2). *Wif1* and *Srd5a2* mRNAs were weakly expressed in 14dC+3dE ventral prostate stroma, and both were noticeably more abundant in 14dC+3dT ventral prostate stroma (Fig. 3, C, D, G, and H). The same trend existed in the other prostate lobes and seminal vesicle (Supplemental Fig. 3). Collectively these results indicate that androgens are required for *Wif1* expression in the intact adult mouse

prostate and are sufficient for reactivating *Wif1* expression during regeneration of the castrated adult mouse prostate.

Exogenous WIF1 protein enhances androgen-dependent prostatic bud formation and basal epithelial cell proliferation

Formation and continued development of *Nkx3-1*-positive prostatic buds requires ARs in UGM (4, 5), but AR-responsive genes mediating this action are largely unknown. We hypothesized that WIF1 enhances AR action by stimulating prostatic bud formation. To test this, E14.5 male UGSs were grown in UGS organ culture media containing DHT and graded concentrations of exogenous recombinant human WIF1 protein (Fig. 4, A–F). Recombinant human WIF1 protein is 93% homologous to the mouse ortholog, and its ability to impair WNT/β-catenin signaling was demonstrated previously in an array of species and tissues including *Xenopus* embryo, chicken heart, and mouse thymus (35–37). Whole-mount ISH was performed as described previously to visualize and quantify the *Nkx3-1*-positive prostatic buds formed per the UGS (24). Exogenous recombinant WIF1 protein elicited a graded increase in the *Nkx3-1*-positive buds (Fig. 4G), which supports the hypothesis that WIF1 enhances androgen-dependent prostatic bud formation.

Because WIF1 enhances prostatic bud formation and developing prostatic buds are comprised of basal epithelium, we next tested the hypothesis that WIF1 enhances androgen-induced UGS basal epithelial cell proliferation. UGS explants were incubated in organ culture media as described above, cut into sagittal sections, and immunofluorescently stained to reveal mitotically active cells (phosphohistone H3 positive, PH3+, *red*) and basal epithelial cells (KRT14+, *green*) (Fig. 5, A–D). Exogenous WIF1 concentrations that significantly increased *Nkx3-1*-positive prostatic bud number (500 ng/ml, 1000 ng/ml; Fig. 4) also significantly increased the mean fraction of $PH3^+KRT14^+$/total $KRT14^+$ cells (Fig. 5E). These results show a pro-proliferative action of WIF1 on UGS basal epithelium.

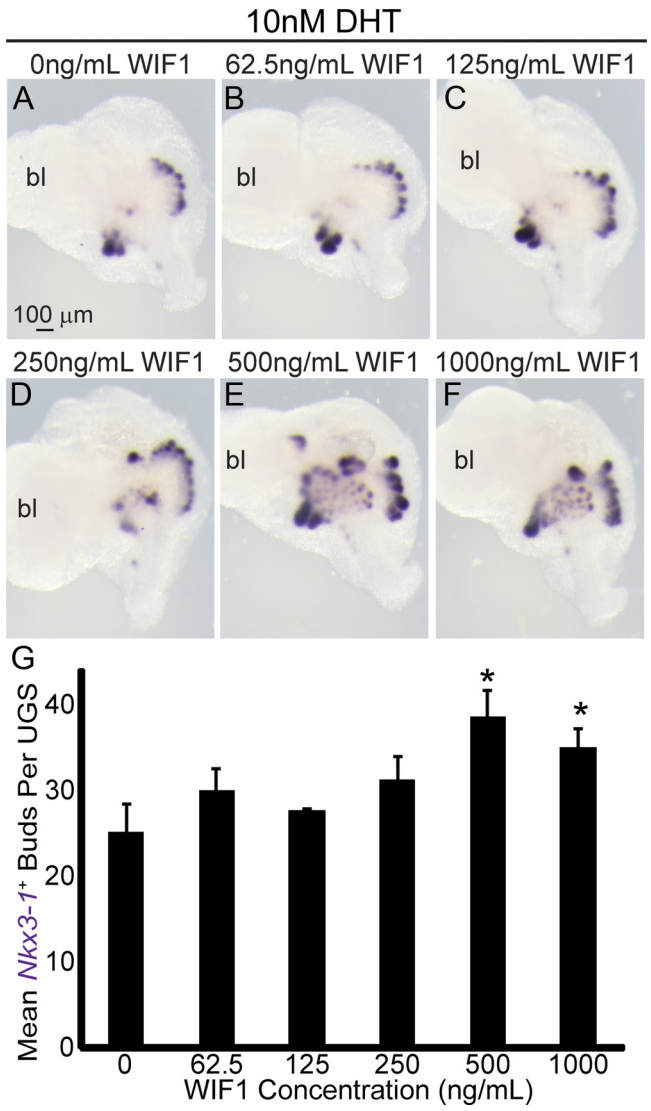

FIG. 4. Exogenous recombinant WIF1 enhances androgen-dependent prostatic bud formation *in vitro*. A–F, E14.5 wild-type male UGSs were cultured for 4 d in the presence of 10 nM DHT and graded concentrations (0–1000 ng/ml) of exogenous recombinant WIF1 protein. Whole-mount tissues were then stained by ISH to visualize and quantify *Nkx3*-1 mRNA-marked prostatic buds (*purple*). G, Results are mean ± SEM (n = 4 litter-independent samples per group). *Asterisks* indicate a significant difference compared with 0 ng/ml WIF1 ($P < 0.05$). bl, Bladder. BM Purple detection time was the same for all samples across experimental groups and was as follows: *Nkx3-1* (21 h).

Exogenous WIF1 does not change the pattern of WNT/β-catenin target genes in prostatic buds

The most widely accepted *Wif1* mechanism of action is functional antagonism of WNT/β-catenin signaling (35, 36, 38). Yet in developing mouse prostate, *Wif1* is expressed in UGM and UGE and overlaps WNT/β-catenin-responsive *Axin2* and *Lef1* (lymphoid enhancer binding factor 1) expression (14, 15, 19). Coexpression of *Wif1* with abundant WNT/β-catenin-responsive mRNA expression would not be predicted if WIF1 functioned as a strong WNT/β-catenin inhibitor in control UGS. We tested whether prostatic bud-enhancing concentrations of exogenous WIF1 protein visibly altered the pattern of WNT/β-catenin-responsive *Axin2* and *Lef1* mRNA within and immediately surrounding prostatic bud tips in which both mRNAs were detected previously (19). E14.5 male UGSs were grown for 4 d in UGS organ culture media containing DHT and graded recombinant WIF1 protein concentrations. ISH was used to visualize *Axin2* and *Lef1* mRNAs. *Axin2* and *Lef1* were detected in prostatic bud

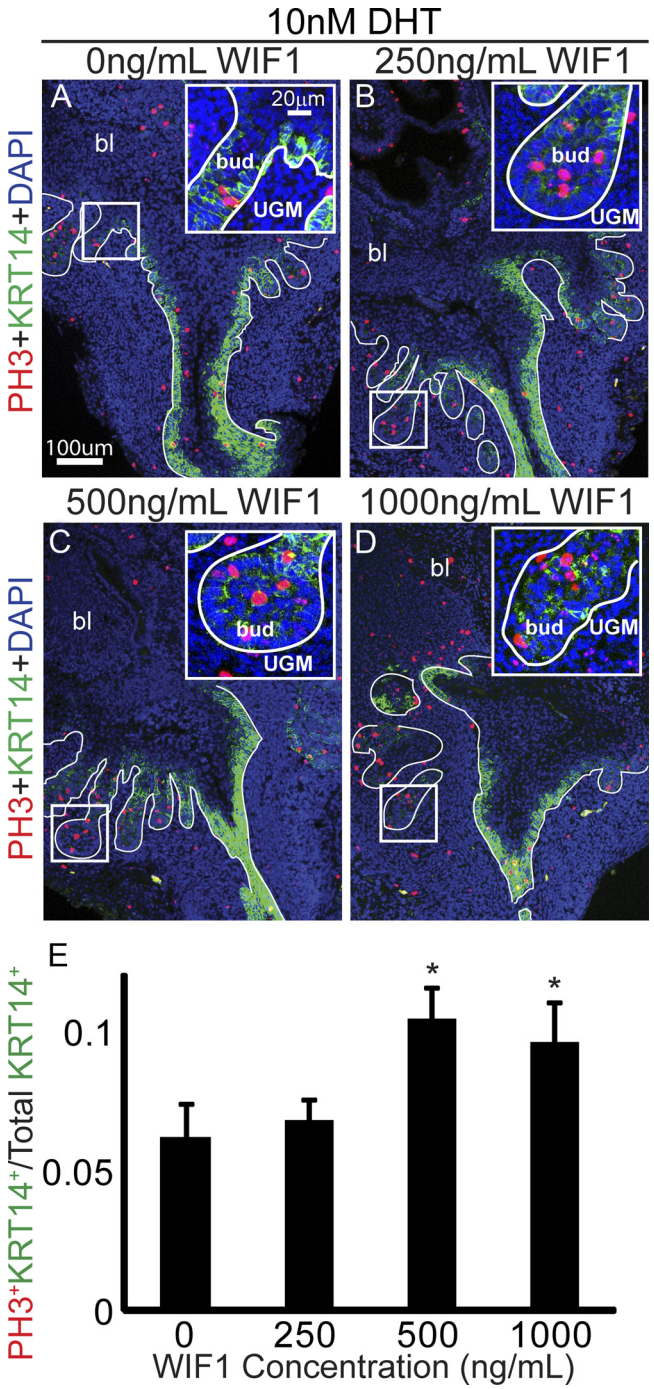

FIG. 5. Exogenous recombinant WIF1 enhances UGS basal epithelial cell proliferation *in vitro*. A–D, E14.5 wild-type male UGSs were cultured for 4 d in the presence of 10 nM DHT and graded concentrations (0–1000 ng/ml) of exogenous recombinant WIF1 protein. Near midsagittal sections (5 μm) were immunofluorescently stained to visualize and count the percentage of KRT14 (*green*)-positive basal epithelial cells with detectable nuclear PH3 (*red*). Cell nuclei were visualized with DAPI (*blue*). E, Results are mean ± SEM (n = 3 litter-independent samples per group). *Asterisks* indicate a significant difference compared with 0 ng/ml WIF1 ($P < 0.05$). *Square insets* represent magnified images. bl, Bladder; bud, prostatic bud. A *white line* marks the interface between UGS epithelium and mesenchyme.

epithelium in all experimental groups, and exogenous recombinant WIF1 did not visibly alter their patterning (Fig. 6). Presence of WNT/β-catenin target genes and *Wif1* at the same time and location during embryonic prostatic development suggests at least two possible mechanisms for prostatic bud enhancement by WIF1: a subtle β-catenin-dependent action we are unable to detect or a β-catenin-independent action.

Exogenous WIF1 is not sufficient to induce prostatic budding in the absence of androgens

To determine whether WIF1 is the only androgen-induced signal needed for prostatic bud formation, E14.5 female UGSs, naïve to high levels of androgens, were cultured for 4 d in androgen-free media containing recombinant WIF1. As a positive control, female UGSs were cultured in media containing 10 nM DHT and no recombinant WIF1. After the culture period, ISH was used to visualize three different prostatic bud-marking mRNAs: *Nkx3-1*, *Wnt10b*, and *Edar* (19, 24, 26). Although *Nkx3-1* is considered the best marker of prostatic buds, *Wnt10b* and *Edar* are additional mRNAs restricted to distal tips of prostatic buds and are not detected in urethral gland buds (19, 24, 26, 32). As expected, DHT induced the formation of *Nkx3-1*-, *Wnt10b*-, and *Edar*-positive prostatic buds in female UGS explants (Fig. 7, D, H, and L, *solid arrowheads*). The only *Nkx3-1* positive buds formed in androgen-free medium were in the ventral UGS region in which small buds were previously shown to form by an androgen-independent mechanism (Fig. 7, A–C, *open arrowheads*) (34). Exogenous WIF1 protein concentrations greater or equal to those that increased prostatic bud number in the presence of androgens (Fig. 4; ≥ 500 ng/ml) did not increase *Nkx3-1*- (Fig. 7, A–C), *Wnt10b*- (Fig. 7, E–G), or *Edar* (Fig. 7, I–K)-positive prostatic bud number in the absence of androgens. Therefore, the formation of large prostatic buds that normally occur in male UGSs likely requires the actions of other androgen-induced factors in collaboration with WIF1.

Prostatic bud number is unaltered in *Wif1* mutant mice

We next assessed whether endogenous *Wif1* is required for androgen-dependent prostatic bud formation *in vivo*. To test this hypothesis, we used a *Wif1* targeted mutant mouse containing a knock-in *lacZ* transgene that disrupts the *Wif1* coding sequence (22). E18.5 male *Wif1* wild-type ($Wif1^{+/+}$) and mutant ($Wif1^{lacZ/lacZ}$) whole-mount UGSs were stained by ISH to visualize and quantify *Nkx3-1*-positive prostatic buds. There were no significant genotypic differences in pattern or number of ventral, anterior, dorsolateral, or total prostatic buds formed (Fig. 8, A–C).

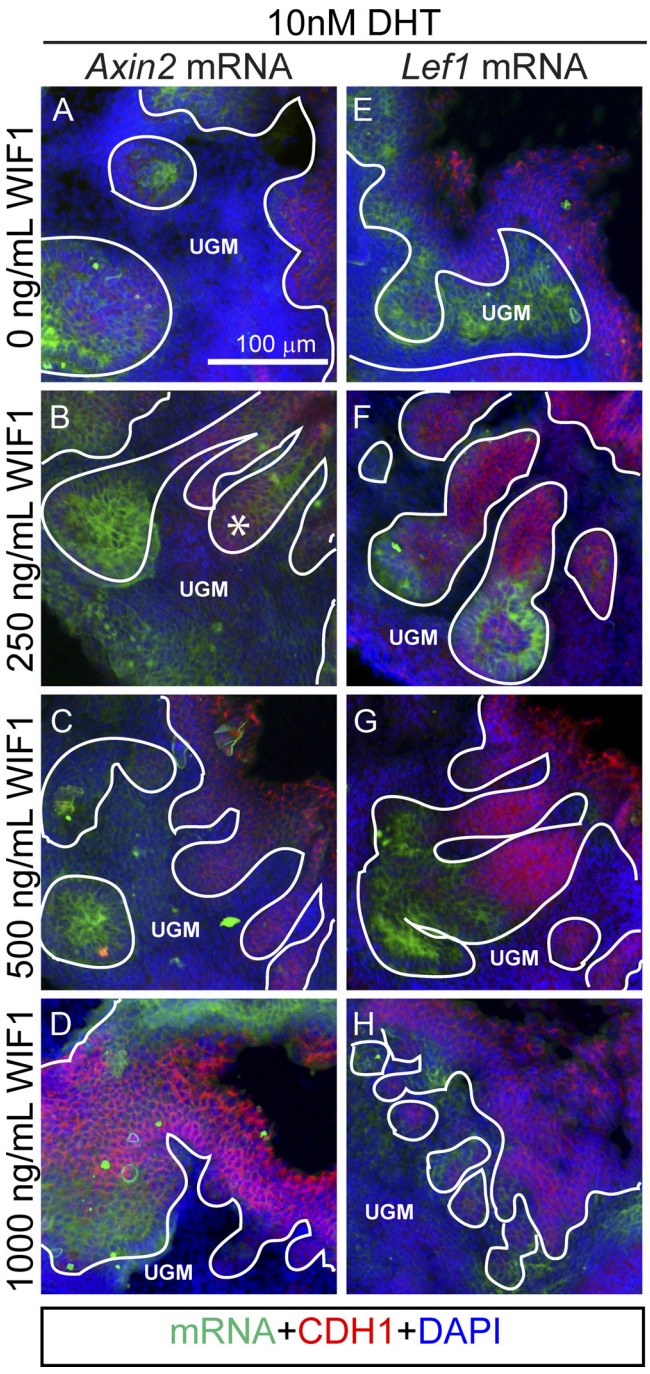

FIG. 6. Exogenous recombinant WIF1 does not visibly alter WNT/β-catenin-responsive *Axin2* and *Lef1* mRNA expression during androgen-dependent prostatic bud formation *in vitro*. E14.5 wild-type male UGSs were cultured for 4 d in the presence of 10 nM DHT and graded concentrations (0–1000 ng/ml) of exogenous recombinant WIF1 protein. Near midsagittal UGS sections (10 μm) were stained by ISH to visualize *Axin2* (A–D) and *Lef1* (E–H) mRNAs (*green*). Sections were then immunofluorescently stained with an antibody against CDH1 (*red*) to label all epithelium and with DAPI (*blue*). Results are representative of three litter-independent samples per treatment group. A *white line* marks the interface between the UGS epithelium and mesenchyme. BM Purple detection time was the same for all samples across the experimental groups and was as follows: *Axin2* (72 h), *Lef1* (72 h).

Therefore, *Wif1* is not required for normal prostatic bud formation. We investigated the possibility that WIF1 acts by a functionally redundant mechanism to promote prostatic bud formation. Specifically, we tested whether *Wif1* mutant mice exhibited a visible compensatory increase in *Sfrp* mRNAs. SFRPs have been identified in the developing prostate and are thought to function in a manner similar to *Wif1* (14, 15, 20). E18.5 *Wif1* mutant and wild-type UGSs were stained by ISH to visualize mRNA expression patterns of *Sfrp1*, *Sfrp2*, *Sfrp3* (also known as *Frzb*), and *Sfrp4* mRNAs. There was no noticeable genotypic difference in *Sfrp1* or *Sfrp4* (results not shown), but there was a noticeably wider band of *Sfrp2* and *Sfrp3* mRNAs in *Wif1* mutant UGSs compared with wild-type (Fig. 8, D–G). Increased expression of *Sfrp2* and *Sfrp3* mRNAs in *Wif1* mutant UGSs suggests balanced WNT signaling is likely to be important in prostatic bud formation.

Discussion

Fetal mouse urethral lamina propria mesenchyme is revealed as a key site of *Wif1* expression and AR action

It has long been known that AR action in UGS stroma is necessary for prostate development (1, 3–5). Yet neither the cellular composition of UGS stroma nor AR activity within UGS stroma is homogeneous (26). This study, in conjunction with other recent studies, refines the subanatomical location of AR action in the developing mouse prostate. Fetal urethral lamina propria mesenchyme, positioned between urethral urothelium and muscularis propria was hypothesized long ago to be an important site of AR action (33). More recent studies identified this subanatomical region as the predominant site of AR-responsive *Srd5a2* expression in mouse (26), rat (39), and male-enriched *Sfrp2* expression in mouse (15). We have now identified *Wif1* as an androgen-responsive mRNA in fetal mouse urethral lamina propria mesenchyme. As the prostate development field moves forward, a focus on this particular fetal prostate subcompartment, which accounts for only about 10% of total UGS stroma, will likely yield information about AR-mediated mechanisms of prostate morphogenesis.

We know very little about prostate stromal cell fate, but identification of fetal mouse urethral lamina propria mesenchymal cells as a key site of AR action may help to close this knowledge gap. For example, epithelial-mesenchymal interactions are crucial for fetal prostate mesenchyme differentiation (40). Whether urethral lamina propria mesenchyme gives rise to smooth muscle or other UGS stromal cell populations or participates in the instructive pattern-

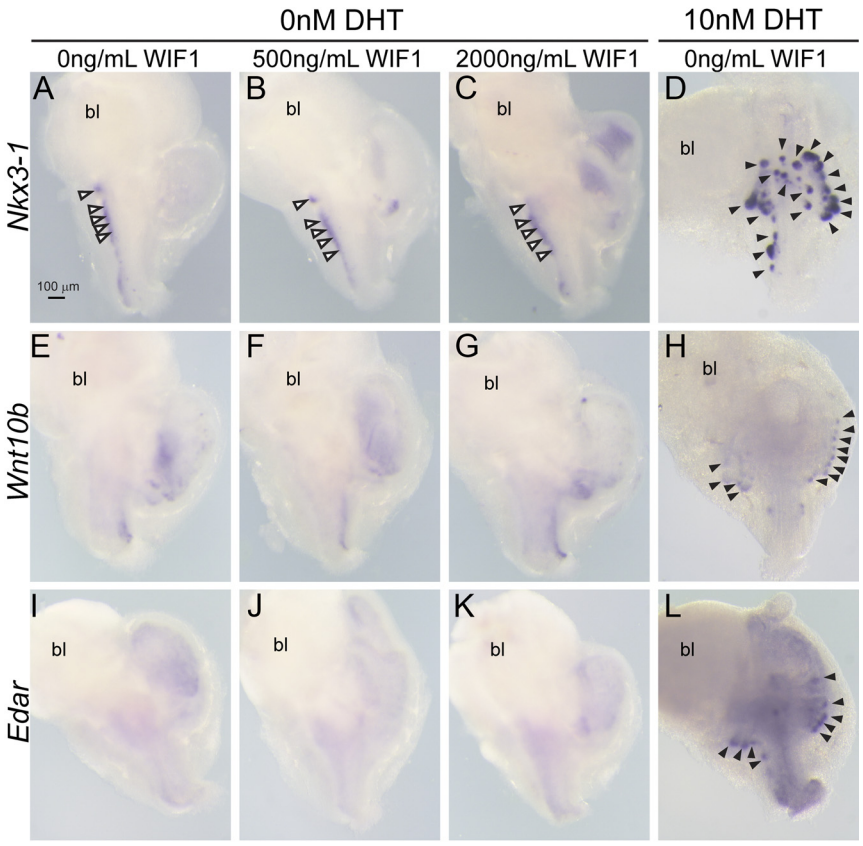

FIG. 7. Exogenous recombinant WIF1 does not stimulate androgen-independent prostatic bud formation *in vitro*. E14.5 wild-type female UGSs were cultured for 4 d in media containing 10 nM DHT (positive control) or in androgen-free media containing exogenous recombinant WIF1 protein. Whole-mount tissues were then stained by ISH to visualize *Nkx3-1* (A–D), *Wnt10b* (E–H), and *Edar* (I–L) mRNA-marked prostatic buds. Results are representative of five litter-independent samples per treatment group. bl, Bladder. A–C, *Open arrowheads* indicate *Nkx3-1*-positive epithelial buds observed in females. D, H, and J, *Solid arrowheads* indicate prostatic and urethral gland buds. BM Purple detection time was the same for all samples across experimental groups and was as follows: *Nkx3-1* (21 h); *Wnt10b* (50 h); *Edar* (36 h).

ing of other UGS stromal constituents (blood vessels, nerves, urethral sphincter skeletal muscle) is unknown. Furthermore, whether urethral lamina propria cells expand clonally during prostatic bud elongation and branching to produce AR-positive periductal mesenchyme cells or whether AR activity is stimulated *de novo* in these cells is unknown. A transgenic mouse that expresses an inducible tag would allow for lineage tracing in urethral lamina propria mesenchyme and would resolve some of these questions.

Wif1 appears to be differently regulated in UGS mesenchyme compared with UGS epithelium

A better understanding of *Wif1* transcriptional regulation during prostate development will shed light on the mechanism of AR-induced prostatic bud formation. We identified *Wif1* in UGM and UGE. Differences in onset, duration, pattern, and androgen-dependence of *Wif1* expression in UGM and UGE suggest distinct *Wif1* transcriptional regulatory mechanisms in these fetal prostate tissue compartments.

In fetal UGE, WNT/β-catenin signaling is more likely than AR signaling to activate *Wif1* transcription. Although AR protein is present in UGE (26, 33), its presence there does not lead to appreciable binding of ligand (33), is expendable for prostatic bud formation (41), and is not needed for *Wif1* expression (Fig. 2). In contrast, β-catenin activity associates with *Wif1* expression in other tissues (42–44), is required for prostatic bud formation (45, 46), and positively regulates the target genes *Axin2* and *Lef1*, which associate spatially and temporally with *Wif1* in UGE (19) (www.gudmap.org).

In fetal UGM, AR signaling is more likely than WNT/β-catenin signaling to activate *Wif1* transcription. AR protein is present in UGM, binds ligand, and is required for prostatic bud formation (1, 3–5). Although WNT/β-catenin-responsive *Axin2* and *Lef1* are present in UGM, both transcripts are detectable at an earlier developmental stage and in a different pattern than *Wif1* (19) (www.gudmap.org), do not persist in UGM as long as *Wif1*, and are not reliant on a high level of androgen signaling in the UGM like *Wif1*. An important future direction of our research is to determine whether *Wif1* transcription in UGM and UGE is regulated directly or indirectly by AR and by β-catenin activities.

Wif1 promotes prostatic bud formation and fetal prostate basal epithelial cell proliferation

A preponderance of evidence supports WIF1 as a suppressor of adult prostate epithelial cell proliferation (47–50). Although few studies have examined WIF1 expression and function during prostate development, Li *et al.* (51) overexpressed WIF1 in UGM, combined UGM with adult bladder epithelium, and grew the tissue recombinants under the kidney capsule of immunocompromised mice. WIF1 overexpression in UGM impaired its ability to reprogram adult bladder epithelium into prostate epithelium, which suggests that abnormally high *Wif1* expression in UGM impairs the instructive signals needed for prostate development (51).

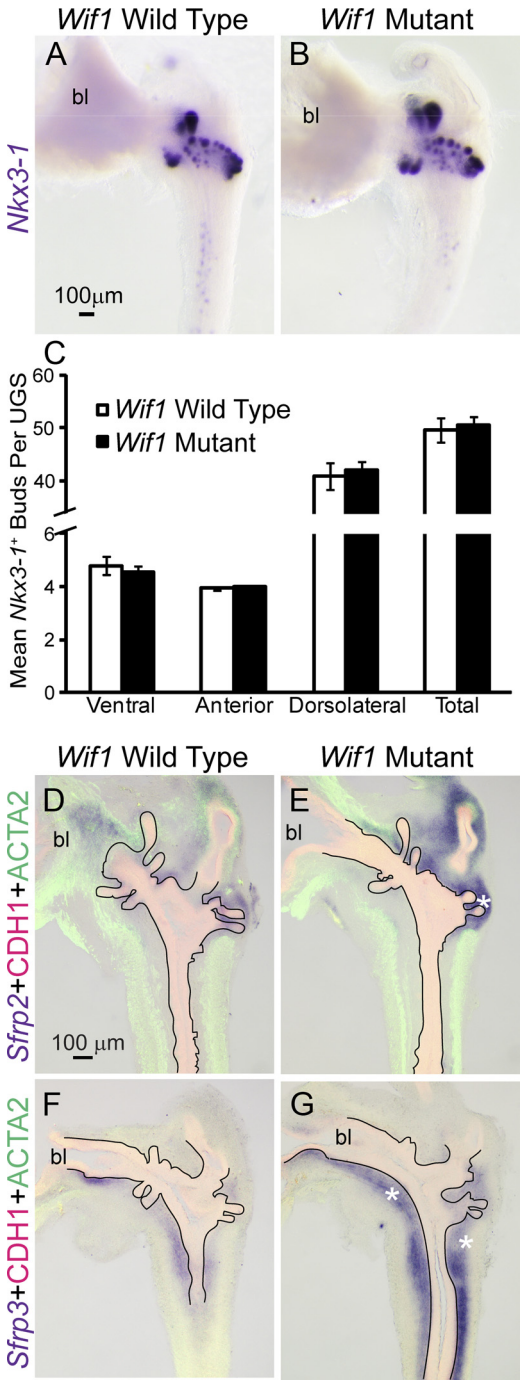

FIG. 8. *Wif1* is not required for normal prostatic bud formation *in vivo*. E18.5 wild-type control (*Wif1*$^{+/+}$) (A) and *Wif1* mutant (*Wif1*$^{lacZ/lacZ}$) male mouse UGSs (B) were stained by ISH to visualize and quantify the number of *Nkx3*-1 mRNA-marked prostatic buds per UGS. C, Results are mean ± SEM (n = 5 litter-independent samples per group). D–G, Near midsagittal sections (50 μm) of E18.5 *Wif1*$^{+/+}$ and *Wif1*$^{lacZ/lacZ}$ male UGSs were stained by ISH to visualize mRNA expression (*purple*) of *Sfrps2* and *Sfrps3*. Sections were then stained by IHC with antibodies against CDH1 (*red*) to label all epithelium and ACTA2 (*green*). Results are representative of two litter-independent samples per genotype. *Asterisks* indicate regions of differential mRNA expression between *Wif1*$^{+/+}$ and *Wif1*$^{lacZ/lacZ}$ male UGSs. bl, Bladder. A *black line* marks the interface between UGS epithelium and mesenchyme. BM Purple detection time was the same for wild-type and mutant UGSs and was as follows: *Nkx3-1* (38 h); *Sfrp2* (5.5 h); *Sfrp3* (63 h).

The results of the current study differ from those described above. We found exogenous recombinant WIF1 protein, at media concentrations of 500-1000 ng/ml, enhanced androgen-dependent mouse prostatic bud formation and basal epithelial cell proliferation (Figs. 4 and 5). Discrepancies in WIF1 action reported in our study *vs.* those described above are likely a function of prostate cell populations present, prostate developmental stages examined, and WIF1 concentrations used. Studies conducted in cell lines (47, 49) or human prostate carcinomas (50) vary in their AR responsiveness, exhibit a cancerous phenotype, and do not fully recapitulate the mesenchymal-epithelial interactions present during prostate development. Additionally, interactions between fetal UGM and adult bladder epithelium under the kidney capsule of an immunocompromised mouse (51) may not be the same as the interactions between intact fetal UGM and UGE in UGS culture medium.

Although we found that exogenous WIF1 protein stimulated prostatic bud formation and UGS basal epithelial cell proliferation, *Wif1* was expendable for normal prostate development (Fig. 8). These results are consistent with observations made by others that *Wif1* is not required for morphogenesis of most mouse tissues (22). A likely possibility is that other genes with a similar function to *Wif1*, such as *Sfrps*, are up-regulated to compensate for the deficient WIF1 activity in *Wif1* mutant UGSs. In support of this possibility, we observed an expanded pattern of *Sfrp2* and *Sfrp3* in *Wif1* mutant UGM compared with wild-type UGM. These results suggest a possible functional redundancy among SFRPs and WIF1 during prostate development.

Possible mechanisms by which WIF1 could enhance fetal prostatic bud formation

One of the most important aspects of the current study is that it reveals WIF1 as one of the first androgen-regulated genes that mediates androgen action during prostate development. An intriguing question raised as a result of our study is how WIF1 enhances prostatic morphogenesis. Although we did not directly answer this question, at least two possible mechanisms should be considered for future investigation: β-catenin-dependent or -independent mechanisms. Even though exogenous WIF1 concentrations that induced prostatic bud formation did not elicit noticeable changes in the pattern of WNT/β-catenin-responsive *Axin2* and *Lef1* mRNAs (Fig. 6), we cannot exclude the possibility that it causes small changes that we were unable to detect. We do not fully understand the concentration-response relationship between β-catenin activity and prostatic bud formation and minor changes in this signaling pathway could account for biologically sig-

nificant changes in prostate development. In chicken proepicardial explant cultures, for example, subtle changes in β-catenin activity in either the positive or negative direction elicit the same response: cardiomyocyte proliferation (36). Therefore, although WNT/β-catenin-responsive *Axin2* and *Lef1* mRNA patterns were not noticeably changed in UGS explants exposed to WIF1, it is possible that we failed to detect subtle or finely localized WIF1-mediated changes in WNT signaling that were important in shaping the pattern and number of prostatic buds formed in the developing mouse UGS.

Finally, it is possible that WIF1 enhances prostatic bud formation by a β-catenin-independent mode of action. Addition of exogenous recombinant WIF1 did not appear to alter WNT/β-catenin target genes *Axin2* and *Lef1* (Fig. 6). Consistent with this finding, abundance of most WNT target genes was unaltered by inappropriately high levels of *Wif1* reported previously in UGM in which *Tgfrb2* was conditionally deleted (51). Vertebrate WIF1 typically functions as an inhibitor of WNT signaling, but *Drosophila* ortholog *shifted* modulates Hedgehog signaling (52). Although it is thought that vertebrate WIF1 does not bind hedgehog, recent evidence suggests that it may be capable of weakly modulating Hedgehog activity (53). WIF1 is also capable of binding connective tissue growth factor *in vitro* independently of its inhibitory action on WNT signaling (54). Whether WIF1 is capable of modulating Hedgehog signaling or whether WIF1 binds other signaling molecules during prostate development is unknown.

Acknowledgments

We thank Jimena Laporta and Laura Hernandez (Department of Dairy Sciences, University of Wisconsin-Madison) for their technical assistance.

Address all correspondence and requests for reprints to: Chad M. Vezina, Department of Comparative Biosciences, School of Veterinary Medicine, University of Wisconsin-Madison, 1656 Linden Drive, Madison, Wisconsin 53706. E-mail: cmvezina@wisc.edu.

This work was supported by the National Institutes of Health Grants DK083425, DK070219, and DK096074 (to C.M.V.), Grants DK091193 and CA140217 (to P.C.M.), and Training Gant T32 ES007015 (to A.M.B.), and National Science Foundation Grant DGE-0718123 (to K.P.K.).

Disclosure Summary: The authors have nothing to disclose.

References

1. **Sugimura Y, Cunha GR, Donjacour AA** 1986 Morphogenesis of ductal networks in the mouse prostate. Biol Reprod 34:961–971
2. **Hayward SW, Cunha GR** 2000 The prostate: development and physiology. Radiol Clin North Am 38:1–14
3. **Cunha GR, Chung LW, Shannon JM, Reese BA** 1980 Stromal-epithelial interactions in sex differentiation. Biol Reprod 22:19–42
4. **Cunha GR** 1973 The role of androgens in the epithelio-mesenchymal interactions involved in prostatic morphogenesis in embryonic mice. Anat Rec 175:87–96
5. **Lasnitzki I, Mizuno T** 1980 Prostatic induction: interaction of epithelium and mesenchyme from normal wild-type mice and androgen-insensitive mice with testicular feminization. J Endocrinol 85:423–428
6. **Memarzadeh S, Xin L, Mulholland DJ, Mansukhani A, Wu H, Teitell MA, Witte ON** 2007 Enhanced paracrine fgf10 expression promotes formation of multifocal prostate adenocarcinoma and an increase in epithelial androgen receptor. Cancer Cell 12:572–585
7. **Cantile M, Kisslinger A, Cindolo L, Schiavo G, D'Antò V, Franco R, Altieri V, Gallo A, Villacci A, Tramontano D, Cillo C** 2005 cAMP induced modifications of HOX D gene expression in prostate cells allow the identification of a chromosomal area involved *in vivo* with neuroendocrine differentiation of human advanced prostate cancers. J Cell Physiol 205:202–210
8. **Sheng T, Li C, Zhang X, Chi S, He N, Chen K, McCormick F, Gatalica Z, Xie J** 2004 Activation of the hedgehog pathway in advanced prostate cancer. Mol Cancer 3:29
9. **Feeley BT, Gamradt SC, Hsu WK, Liu N, Krenek L, Robbins P, Huard J, Lieberman JR** 2005 Influence of BMPs on the formation of osteoblastic lesions in metastatic prostate cancer. J Bone Miner Res 20:2189–2199
10. **Pienta KJ, Nguyen NM, Lehr JE** 1993 Treatment of prostate cancer in the rat with the synthetic retinoid fenretinide. Cancer Res 53:224–226
11. **Lai KP, Yamashita S, Vitkus S, Shyr CR, Yeh S, Chang C** 2012 Suppressed prostate epithelial development with impaired branching morphogenesis in mice lacking stromal fibromuscular androgen receptor. Mol Endocrinol 26:52–66
12. **Niu Y, Altuwaijri S, Lai KP, Wu CT, Ricke WA, Messing EM, Yao J, Yeh S, Chang C** 2008 Androgen receptor is a tumor suppressor and proliferator in prostate cancer. Proc Natl Acad Sci USA 105:12182–12187
13. **Yamamoto H, Oue N, Sato A, Hasegawa Y, Yamamoto H, Matsubara A, Yasui W, Kikuchi A** 2010 Wnt5a signaling is involved in the aggressiveness of prostate cancer and expression of metalloproteinase. Oncogene 29:2036–2046
14. **Pritchard CC, Nelson PS** 2008 Gene expression profiling in the developing prostate. Differentiation 76:624–640
15. **Zhang TJ, Hoffman BG, Ruiz de Algara T, Helgason CD** 2006 Sage reveals expression of wnt signaling pathway members during mouse prostate development. Gene Expr Patterns 6:310–324
16. **Parker MG, Mainwaring WI** 1977 Effects of androgens on the complexity of poly(a) RNA from rat prostate. Cell 12:401–407
17. **Parker MG, White R, Williams JG** 1980 Cloning and characterization of androgen-dependent mRNA from rat ventral prostate. J Biol Chem 255:6996–7001
18. **Thomsen MK, Butler CM, Shen MM, Swain A** 2008 Sox9 is required for prostate development. Dev Biol 316:302–311
19. **Mehta V, Abler LL, Keil KP, Schmitz CT, Joshi PS, Vezina CM** 2011 Atlas of wnt and r-spondin gene expression in the developing male mouse lower urogenital tract. Dev Dyn 240:2548–2560
20. **Joesting MS, Perrin S, Elenbaas B, Fawell SE, Rubin JS, Franco OE, Hayward SW, Cunha GR, Marker PC** 2005 Identification of sfrp1 as a candidate mediator of stromal-to-epithelial signaling in prostate cancer. Cancer Res 65:10423–10430
21. **Wang BE, Wang XD, Ernst JA, Polakis P, Gao WQ** 2008 Regulation of epithelial branching morphogenesis and cancer cell growth of the prostate by wnt signaling. PLoS One 3:e2186
22. **Kansara M, Tsang M, Kodjabachian L, Sims NA, Trivett MK, Ehrich M, Dobrovic A, Slavin J, Choong PF, Simmons PJ, Dawid IB,**

Thomas DM 2009 Wnt inhibitory factor 1 is epigenetically silenced in human osteosarcoma, and targeted disruption accelerates osteosarcomagenesis in mice. J Clin Invest 119:837–851
23. **Abler LL, Mehta V, Keil KP, Joshi PS, Flucus CL, Hardin HA, Schmitz CT, Vezina CM** 2011 A high throughput in situ hybridization method to characterize mrna expression patterns in the fetal mouse lower urogenital tract. J Vis Exp 54:2912
24. **Keil KP, Mehta V, Abler LL, Joshi PS, Schmitz CT, Vezina CM** 2012 Visualization and quantification of mouse prostate development by *in situ* hybridization. Differentiation 84:232–239
25. **Vezina CM, Allgeier SH, Fritz WA, Moore RW, Strerath M, Bushman W, Peterson RE** 2008 Retinoic acid induces prostatic bud formation. Dev Dyn 237:1321–1333
26. **Abler LL, Keil KP, Mehta V, Joshi PS, Schmitz CT, Vezina CM** 2011 A high-resolution molecular atlas of the fetal mouse lower urogenital tract. Dev Dyn 240:2364–2377
27. **Livak KJ, Schmittgen TD** 2001 Analysis of relative gene expression data using real-time quantitative PCR and the 2[-ΔΔC(T)] method. Methods 25:402–408
28. **Witte F, Dokas J, Neuendorf F, Mundlos S, Stricker S** 2009 Comprehensive expression analysis of all Wnt genes and their major secreted antagonists during mouse limb development and cartilage differentiation. Gene Expr Patterns 9:215–223
29. **Vezina CM, Allgeier SH, Moore RW, Lin TM, Bemis JC, Hardin HA, Gasiewicz TA, Peterson RE** 2008 Dioxin causes ventral prostate agenesis by disrupting dorsoventral patterning in developing mouse prostate. Toxicol Sci 106:488–496
30. **Lin TM, Rasmussen NT, Moore RW, Albrecht RM, Peterson RE** 2003 Region-specific inhibition of prostatic epithelial bud formation in the urogenital sinus of c57bl/6 mice exposed in utero to 2,3,7,8-tetrachlorodibenzo-*p*-dioxin. Toxicol Sci 76:171–181
31. **Matsui D, Sakari M, Sato T, Murayama A, Takada I, Kim M, Takeyama K, Kato S** 2002 Transcriptional regulation of the mouse steroid 5α-reductase type II gene by progesterone in brain. Nucleic Acids Res 30:1387–1393
32. **Bhatia-Gaur R, Donjacour AA, Sciavolino PJ, Kim M, Desai N, Young P, Norton CR, Gridley T, Cardiff RD, Cunha GR, Abate-Shen C, Shen MM** 1999 Roles for nkx3.1 in prostate development and cancer. Genes Dev 13:966–977
33. **Takeda H, Lasnitzki I, Mizuno T** 1987 Change of mosaic pattern by androgens during prostatic bud formation in XTfm/X+ heterozygous female mice. J Endocrinol 114:131–137
34. **Allgeier SH, Lin TM, Moore RW, Vezina CM, Abler LL, Peterson RE** 2010 Androgenic regulation of ventral epithelial bud number and pattern in mouse urogenital sinus. Dev Dyn 239:373–385
35. **Hsieh JC, Kodjabachian L, Rebbert ML, Rattner A, Smallwood PM, Samos CH, Nusse R, Dawid IB, Nathans J** 1999 A new secreted protein that binds to wnt proteins and inhibits their activities. Nature 398:431–436
36. **Buermans HP, van Wijk B, Hulsker MA, Smit NC, den Dunnen JT, van Ommen GB, Moorman AF, van den Hoff MJ, 't Hoen PA** 2010 Comprehensive gene-expression survey identifies wif1 as a modulator of cardiomyocyte differentiation. PLoS One 5:e15504
37. **Mathieu YD** 2006 Identification of novel genes involved in the commitment of endodermal cells to the thymic epithelial cell fate. Dissertation, University of Basel (http://edoc.unibas.ch/diss/DissB_7888)
38. **Surmann-Schmitt C, Widmann N, Dietz U, Saeger B, Eitzinger N, Nakamura Y, Rattel M, Latham R, Hartmann C, von der Mark H, Schett G, von der Mark K, Stock M** 2009 Wif-1 is expressed at cartilage-mesenchyme interfaces and impedes wnt3a-mediated inhibition of chondrogenesis. J Cell Sci 122:3627–3637
39. **Berman DM, Tian H, Russell DW** 1995 Expression and regulation of steroid 5α-reductase in the urogenital tract of the fetal rat. Mol Endocrinol 9:1561–1570
40. **Cunha GR** 2008 Mesenchymal-epithelial interactions: past, present, and future. Differentiation 76:578–586
41. **Cunha GR, Donjacour AA, Cooke PS, Mee S, Bigsby RM, Higgins SJ, Sugimura Y** 1987 The endocrinology and developmental biology of the prostate. Endocr Rev 8:338–362
42. **Reguart N, He B, Xu Z, You L, Lee AY, Mazieres J, Mikami I, Batra S, Rosell R, McCormick F, Jablons DM** 2004 Cloning and characterization of the promoter of human wnt inhibitory factor-1. Biochem Biophys Res Commun 323:229–234
43. **Zirn B, Samans B, Wittmann S, Pietsch T, Leuschner I, Graf N, Gessler M** 2006 Target genes of the wnt/β-catenin pathway in Wilms tumors. Genes Chromosomes Cancer 45:565–574
44. **Martinez G, Wijesinghe M, Turner K, Abud HE, Taketo MM, Noda T, Robinson ML, de Iongh RU** 2009 Conditional mutations of β-catenin and APC reveal roles for canonical Wnt signaling in lens differentiation. Invest Ophthalmol Vis Sci 50:4794–4806
45. **Simons BW, Hurley PJ, Huang Z, Ross AE, Miller R, Marchionni L, Berman DM, Schaeffer EM** 2012 Wnt signaling through beta-catenin is required for prostate lineage specification. Dev Biol 371:246–255
46. **Schmitz C, Mehta V, Joshi P, Abler L, Keil K, Vezina C** Requirement for β-catenin in prostatic bud formation. Proc Society for Basic Urologic Research Fall Symposium, Las Vegas, NV, November 11, 2011, p 163 (Abstract 66)
47. **Yee DS, Tang Y, Li X, Liu Z, Guo Y, Ghaffar S, McQueen P, Atreya D, Xie J, Simoneau AR, Hoang BH, Zi X** 2010 The Wnt inhibitory factor 1 restoration in prostate cancer cells was associated with reduced tumor growth, decreased capacity of cell migration and invasion and a reversal of epithelial to mesenchymal transition. Mol Cancer 9:162
48. **Costa VL, Henrique R, Ribeiro FR, Carvalho JR, Oliveira J, Lobo F, Teixeira MR, Jerónimo C** 2010 Epigenetic regulation of wnt signaling pathway in urological cancer. Epigenetics 5:343–351
49. **Ohigashi T, Mizuno R, Nakashima J, Marumo K, Murai M** 2005 Inhibition of Wnt signaling downregulates AKT activity and induces chemosensitivity in PTEN-mutated prostate cancer cells. Prostate 62:61–68
50. **Wissmann C, Wild PJ, Kaiser S, Roepcke S, Stoehr R, Woenckhaus M, Kristiansen G, Hsieh JC, Hofstaedter F, Hartmann A, Knuechel R, Rosenthal A, Pilarsky C** 2003 Wif1, a component of the wnt pathway, is down-regulated in prostate, breast, lung, and bladder cancer. J Pathol 201:204–212
51. **Li X, Wang Y, Sharif-Afshar AR, Uwamariya C, Yi A, Ishii K, Hayward SW, Matusik RJ, Bhowmick NA** 2009 Urothelial transdifferentiation to prostate epithelia is mediated by paracrine TGF-β signaling. Differentiation 77:95–102
52. **Glise B, Miller CA, Crozatier M, Halbisen MA, Wise S, Olson DJ, Vincent A, Blair SS** 2005 Shifted, the drosophila ortholog of Wnt inhibitory factor-1, controls the distribution and movement of hedgehog. Dev Cell 8:255–266
53. **Avanesov A, Honeyager SM, Malicki J, Blair SS** 2012 The role of glypicans in Wnt inhibitory factor-1 activity and the structural basis of Wif1's effects on Wnt and hedgehog signaling. PLoS Genet 8:e1002503
54. **Surmann-Schmitt C, Sasaki T, Hattori T, Eitzinger N, Schett G, von der Mark K, Stock M** 2012 The Wnt antagonist Wif-1 interacts with CTGF and inhibits CTGF activity. J Cell Physiol 227:2207–2216